CHAPTER IV
RESULTS AND DISCUSSION

In this study, pure Ultem®1000 membrane and its mixed matrix membranes (MMMs) are designated as follows:

1. Pure Ultem Membrane (UTM)
2. 10 wt% Basolite™ C300/Ultem MMMs (10M199-U MMM)
3. 20 wt% Basolite™ C300/Ultem MMMs (20M199-U MMM)
4. 30 wt% Basolite™ C300/Ultem MMMs (30M199-U MMM)
5. 10 wt% Basolite® Z1200/Ultem MMMs (10ZIF8-U MMM)
6. 20 wt% Basolite® Z1200/Ultem MMMs (20ZIF8-U MMM)

All types of membranes were composed of 13 wt% Ultem polymer as a continuous matrix phase with a range of MOF-199 loadings from 10 wt% to 30 wt% or ZIF-8 loadings from 10 wt% to 20 wt%. This section presents gas permeance results as well as the characterization of resulting MMMs fabricated. In addition, the experimental results obtained from single gas permeation measurements are discussed for both UTM and its MMMs.

4.1 Membrane Characterization

UTM and MOF-U MMMs were characterized by Scanning Electron Microscopy (SEM). The cross-section morphologies of prepared membranes are shown in Figure 4.1. Scanning electron microscopy (SEM) was performed using a Hitachi TM3000 microscope. Samples were prepared by the freeze-fracture of the membrane and subsequent sputter-coating with a thin layer of platinum to reduce sample charging under the electron beam.

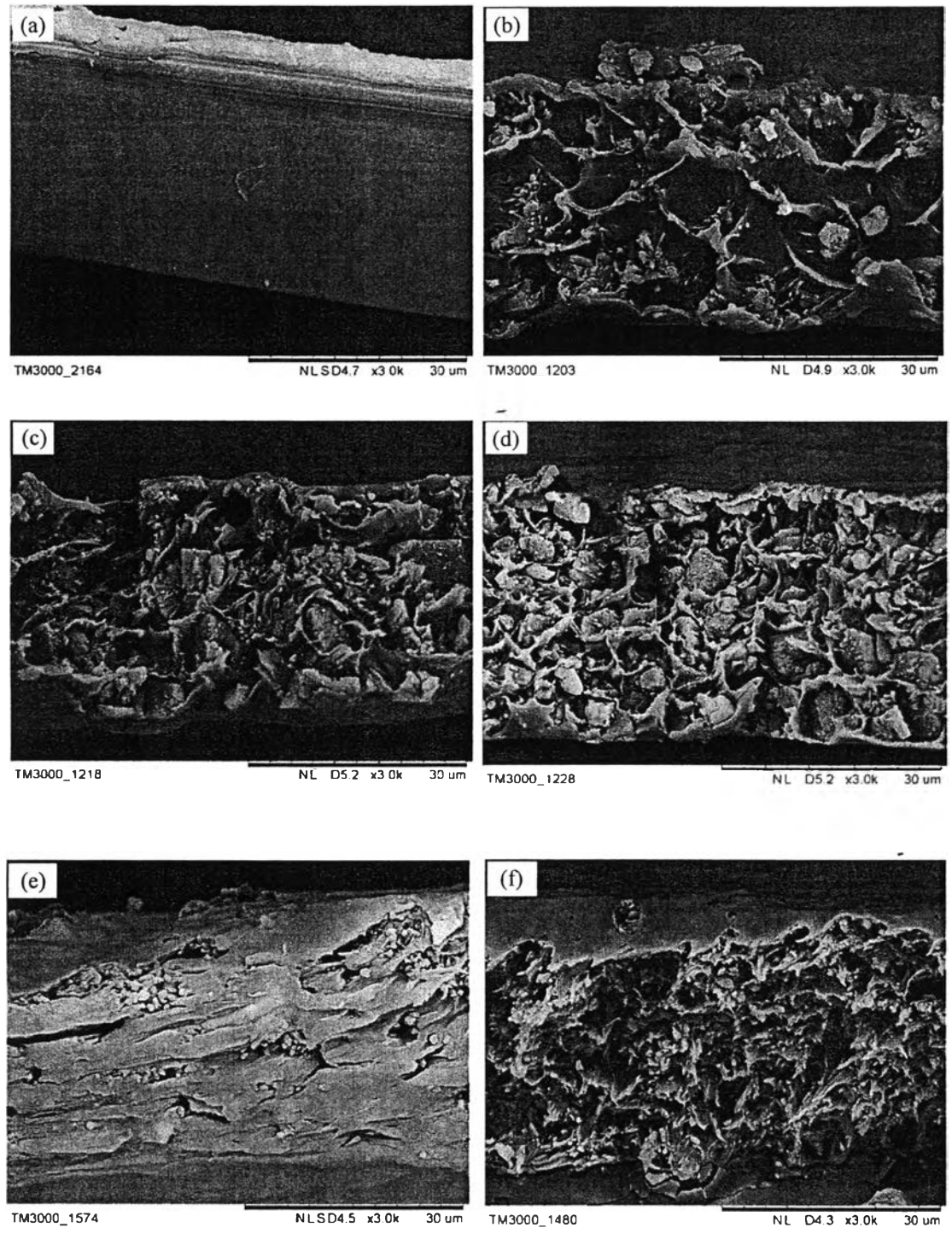

Figure 4.1 SEM images of the cross-sectional (a) UTM, (b) 10 M199-U MMM, (c) 20 M199-U MMM, (d) 30 M199-U MMM, (e) 10 ZIF8-U MMM, and (f) 20 ZIF8-U MMM.

Figure 4.1 (a) shows SEM image of the cross-sectional UTM which can be observed homogeneity of Ultem polymer with the membrane thickness of ca. 30 μm. However, the inhomogeneity at the top of membrane might be caused by the fast evaporation of NMP, which occurred during the membrane casting. From Figures 4.1 (b) and (c), the membranes containing 10 wt% and 20 wt% of MOF-199, respectively, show small aggregation of MOF-199 particles at the surface of membrane, in contrast to the 30 M199-U MMM, shown in Figure 4.1 (d), which shows a good distribution of MOF-199 nanoparticles and good adhesion between the polymer and MOF interface.

As shown in Figure 4.1 (e), the membrane containing 10 wt% ZIF-8 shows poor dispersion of ZIF-8 nanoparticles and consequently poor adhesion at the MOF-polymer interface. Such aggregation is consistent with the results reported by Yang *et al.* (2011) and Liu *et al.* (2011). At higher loading of 20 wt% ZIF-8, the ZIF-8 particles show dispersed better than at 10 wt% ZIF-8 loading. However, as compared to M199-U MMMs, the membranes containing ZIF-8 had more non-selective voids in MMMs. Apart from the ZIF8-U MMMs, the avoidance of larger non-selective voids in the MMMs has been accomplished by choosing an appropriate polymer as the matrix in combination with a suitable membrane fabrication process (Ploegmakers *et al.*, 2013). The combination of polar MOF-199 inside a polar UTM allows for polar interactions, thereby improving the polymer-MOF interfacial adhesion. Also, the gradual addition of the Ultem powder to the MOF solution during the membrane fabrication process prevents a large agglomeration of the MOF particles and the Ultem polymer.

4.2 Single Gas Permeability Measurements

4.2.1 Pure Ultem Dense Membrane

The permeation properties of UTM were evaluated using pure gas permeation measurements according to the sequential testing application of nitrogen (N_2), methane (CH_4), and carbon dioxide (CO_2). In this study, the nitrogen gas was used as both a tested gas and a carrier gas in order to remove any gases or other contaminants inside the pore of the tested membranes as well as to minimize the

effect of CO_2 plasticization. Gas permeance and gas selectivity determined from a flow rate of each gas at steady state through the UTM at room temperature and pressures of 50 psi and 100 psi are presented in Figures 4.2 and 4.3, respectively.

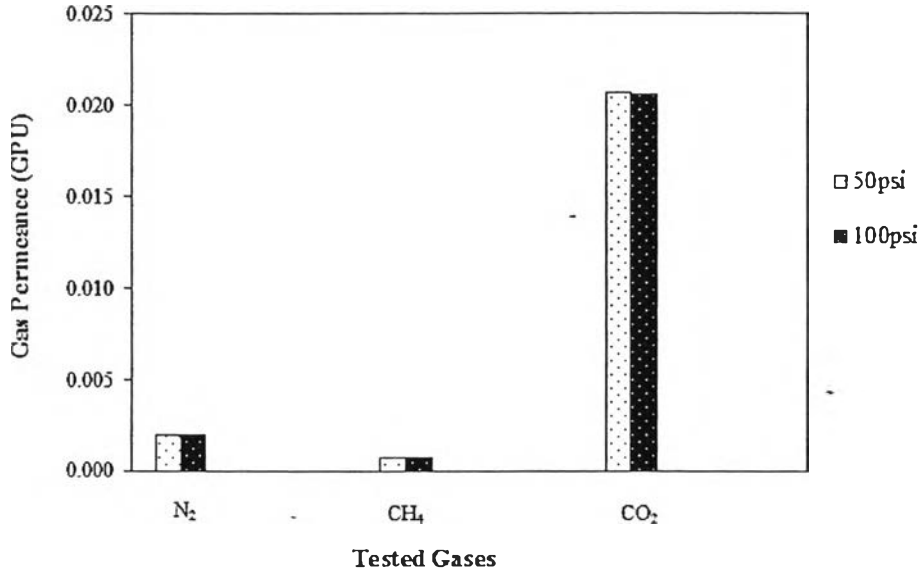

Figure 4.2 Gas permeance of the UTM at pressures of 50 psi and 100 psi.

As shown in Figure 4.2, for the UTM, CO_2 possesses the highest gas permeance followed by N_2 and CH_4 in sequence. The values of CO_2 permeance at pressures of 50 psi and 100 psi were 0.02065 GPU and 0.02063 GPU, respectively, while those of N_2 permeance were respectively 0.00199 GPU and 0.00201 GPU, and those of CH_4 permeance were 0.0074 GPU and 0.0075 GPU, respectively. The results were conformed to the principle of solution-diffusion mechanisms for dense membranes (Zang *et al.*, 2013). In a solution-diffusion model, an increase in gas permeation rate is regulated by the polymer molecular structure that allows preferential passing of certain gas molecules based on their sizes, normally represented by their kinetic diameters as shown in Table 4.1.

Table 4.1 Kinetic diameters of tested gases (Suntiworawut *et al.*, 2009)

Gas	Kinetic diameter (Å)
CO_2	3.30
N_2	3.64
CH_4	3.80

The CO_2/CH_4 and CO_2/N_2 selectivities of UTM at pressures of 50 psi and 100 psi are shown in Figure 4.3. Due to the condensable nature of CO_2 and its good interaction with the polar segments of Ultem polymer, UTM is more selective to CO_2 than both CH_4 and N_2 where its values of CO_2/CH_4 selectivity were 27.72 and 27.70 and its values of CO_2/N_2 selectivity were 10.40 and 10.27 at pressures of 50 psi and 100 psi, respectively. The results were in good agreement with those obtained by Vu *et al.* (2003) and Suntiworawut *et al.* (2009).

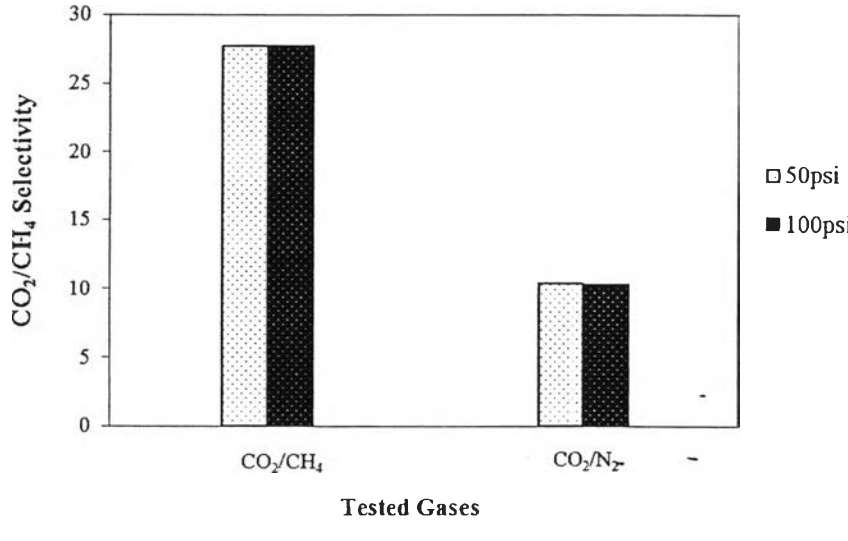

Figure 4.3 Gas selectivity of the UTM at pressures of 50 psi and 100 psi.

4.2.2 Metal Organic Frameworks-Ultem Mixed Matrix Membranes

The permeances of CO_2, N_2, and CH_4 at steady state through the UTM and MOF MMMs at room temperature and pressures of 50 psi and 100 psi are presented in Figures 4.4 and 4.5, respectively.

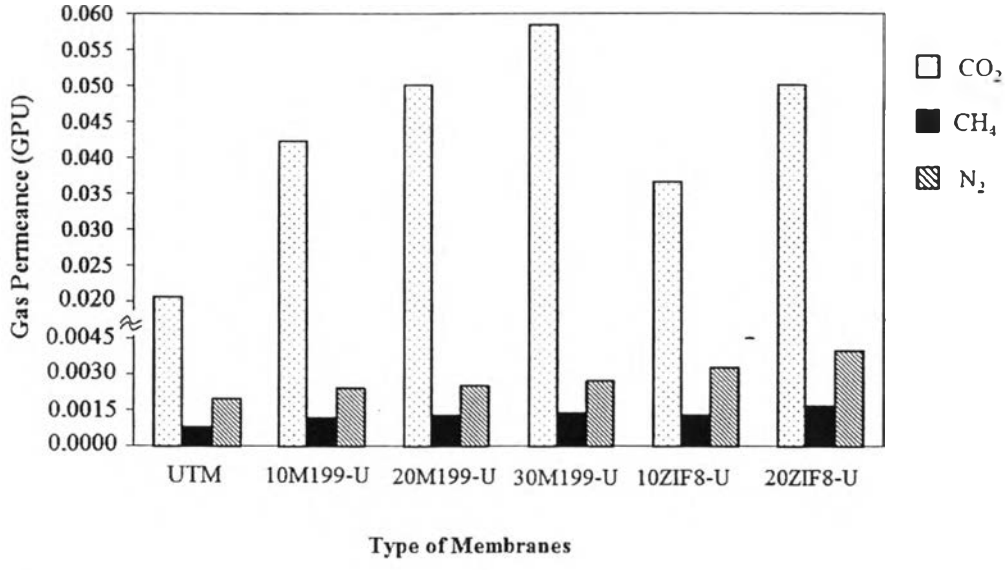

Figure 4.4 Permeances of the tested gases for the fabricated membranes at the pressure of 50 psi.

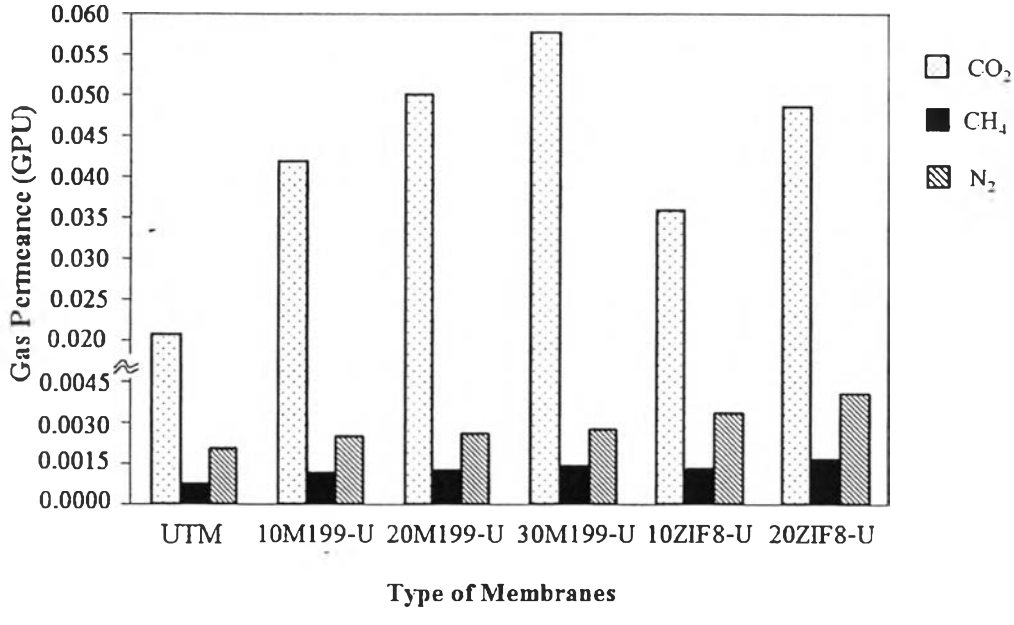

Figure 4.5 Permeances of the tested gases for the fabricated membranes at the pressure of 100 psi.

The selectivities of CO_2/CH_4 and CO_2/N_2 determined from gas permeance for the UTM and MOF-U MMMs at room temperature and pressures of 50 psi and 100 psi are presented in Figures 4.6 and 4.7, respectively.

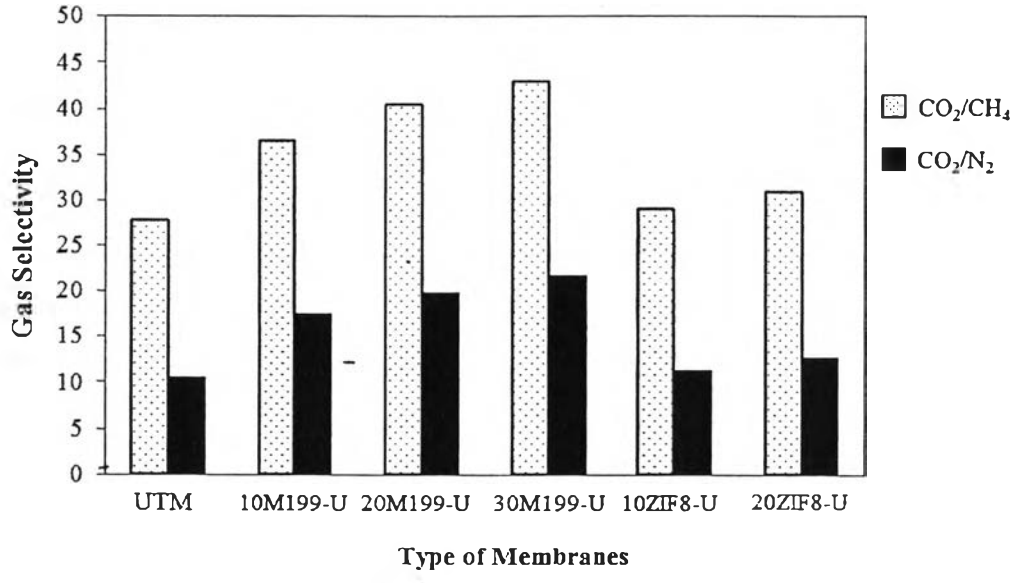

Figure 4.6 CO_2/CH_4 and CO_2/N_2 ideal selectivities of the fabricated membranes at the pressure of 50 psi.

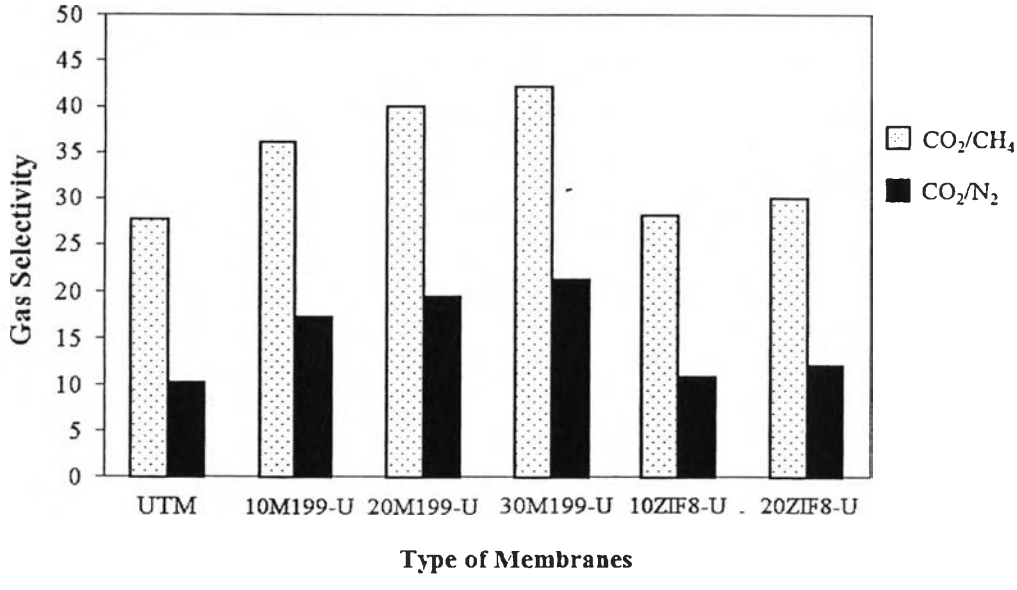

Figure 4.7 CO_2/CH_4 and CO_2/N_2 ideal selectivities of the fabricated membranes at the pressure of 100 psi.

The enhancement of gas permeance and ideal gas selectivity were clearly observed when incorporating the MOFs into UTM as shown in Figures 4.4 – 4.7. For M199-U MMMs, the gas permeances were significantly increased with increasing MOF loading. As compared to the densed membrane, increases to 284% in CO_2 permeance (From 0.021 GPU to 0.059 GPU), to 154% in N_2 permeance (From 0.00199 GPU to 0.00306 GPU), and to 184% in CH_4 permeance (From 0.00074 GPU to 0.00136 GPU) were observed for 30 M199-U MMM. Moreover, a significant increase in CO_2/CH_4 selectivity (From 27 to 43) was observed for the 30 M199-U MMM. Similarly, CO_2/N_2 selectivity was increased with increasing MOF loading even though it was less pronounced than that of CO_2/CH_4. This might be due to two main reasons. Firstly, the size exclusion, related to the dimension and shape of the framework pores. The MOF-199 is a three-dimensional network with a zeolite-like structure consisting of the tetrahedral and main channels connected by triangular window of 3.5 Å in diameter which allows the gas molecules smaller than that of channels passing through. Secondly, the CO_2-selective properties of this MOF would play a role. The MOF-199 exhibits unsaturated metal sites for which CO_2 is selectively attracted towards these unsaturated Cu atoms in the MOF-199 frameworks over CH_4 or N_2 as reported by Nik *et al.* (2012).

In case of ZIF8-U MMMs, permeances of all tested gases were significantly higher than the densed membrane at a higher ZIF-8 loading without a significant improvement in CO_2/CH_4 selectivity. As compared to the densed membrane, the 20 ZIF8-U MMM could improve the CO_2 permeance up to 243% (from 0.021 GPU to 0.05 GPU) while the CO_2/CH_4 showed a slight increase of 8% (from 27 to 30). Since the crystallographic pore aperture of ZIF-8 crystal is ca. 3.4 Å, it would allow the transport of gas molecules with the smaller kinetic diameter, such as CO_2, blocking the larger molecules including N_2 and CH_4. However, increases in both N_2 and CH_4 permeances might be due to the defect interface between the ZIF-8 particles and Ultem polymer, called the sieve in a cage morphology, as also observed in the literatures (Dai *et al.*, 2012 and Song *et al.*, 2012).

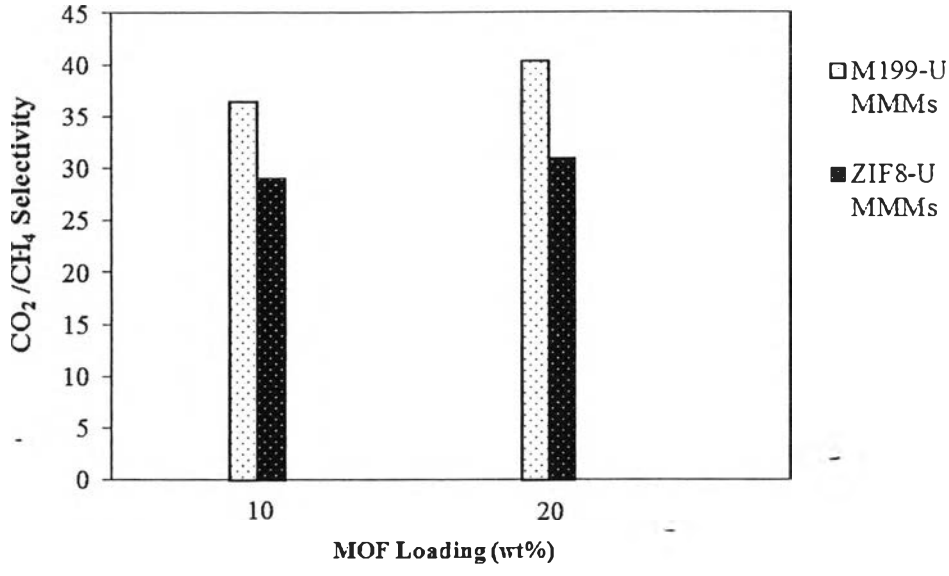

Figure 4.8 Comparison of CO_2/CH_4 selectivity between M199-U MMMs and ZIF8-U MMMs at pressure of 50 psi.

Figure 4.8 shows a comparison of CO_2/CH_4 selectivity between M199-U MMMs and ZIF8-U MMMs. The M199-U MMMs showed a higher CO_2/CH_4 selectivity than the ZIF-Ultem MMMs for both loadings at 10 wt% and 20 wt%. This is might be due to the sieve in a cage morphology for ZIF-8 particles and Ultem polymer which allows all gases passing through it easily. Also, some minor voids were observed in the SEM image shown in Figures 4.1 (e) and (f). This indicated that the compatibility between MOF particle and Ultem polymer of ZIF-8 was less than that of MOF-199 and therefore could have a reduced interaction with the Ultem polymer.

4.3 Effect of Pressure

Since the pressure differences across a membrane at 50 psi and 100 psi were employed for investigating the effect of pressure on membrane performance, gas permeances for the membrane fabricated under different testing pressures are shown in Figures 4.4 and 4.5.

An increase in differential pressure across a membrane resulted in an insignificant decrease in CO_2/CH_4 selectivity as observed for individual membranes in the pressure range of 50 psi to 100 psi. However, decreases in CO_2 permeance and

CO_2/CH_4 selectivity at a higher pressure might be due to the dual-mode behavior of glassy polymers because Ultem is a glassy polymer. Such a behavior can be described on which the permeability first decreased with increasing the CO_2 pressure and then increased with further increasing CO_2 pressure. The increase in permeability with increasing pressure was due to the plasticizing effect (Staudt-Bickel and Koros, 1998). However, the studied pressure of 100 psi was not really high enough to cause the plasticizing effect. On the other hand, the permeances of N_2 and CH_4 remained constant.

4.4 The Maxwell Model

The Maxwell model is usually used to predict the transport properties of gases through MMMs. This well-known model was initially presented by Maxwell in 1873 (Song *et al.*, 2012). Ideally, the model is applicable to diluted suspensions of spherical particles in a matrix without consideration of non-ideal cases, such as the particle size distribution, shape, interfacial voids, aggregation of particles, pore blockage, and rigidification of surrounding polymer chains. However, Chiew and Glandt (1983) proposed an extension equation to consider the interaction between particles and continuous media including the interaction between particles and the particle size. They found that although the particle size was neglected in the Maxwell equation compared with the mean distance within the particles, the interaction between the particles and the continuous media was considered at low amount of particle loading. Moreover, the Maxwell model equation was also easy to calculate than other models. Therefore, this model was chosen to predict the effective permeability for the MMMs. The Maxwell model can be written as follows:

$$P_{eff} = P_c\left[\frac{P_d + 2P_c - 2\phi_d(P_c - P_d)}{P_d + 2P_c + \phi_d(P_c - P_d)}\right] \qquad 4.1$$

where P_{eff} is the effective permeability of the composite membrane, P_c and P_d are the permeability of the continuous phase (polymer) and dispersed phase (MOF),

respectively, and ϕ_d is the volume fraction of dispersed phase. With the permeability, the ideal selectivity of gases could also be predicted.

The gas permeation values of pure ZIF-8 used in the model were recalculated form the pure gas permeation data reported by Bux *et al.* (2009). For the gas permeation values of MOF-199, it was not reported in any literatures. However, to predict the gas permeances by the Maxwell model, the gas permeation values of pure ZIF-8 was used instead of those values of pure MOF-199. Because the values of gas permeance based on the Maxwell model which were obtained by trial and error in wide range were not shown a significant change.

Figures 4.9, 4.10, and 4.11 present the permeances of CO_2, CH_4, and N_2 obtained from the experiment and by model for MOF-U MMMs, respectively.

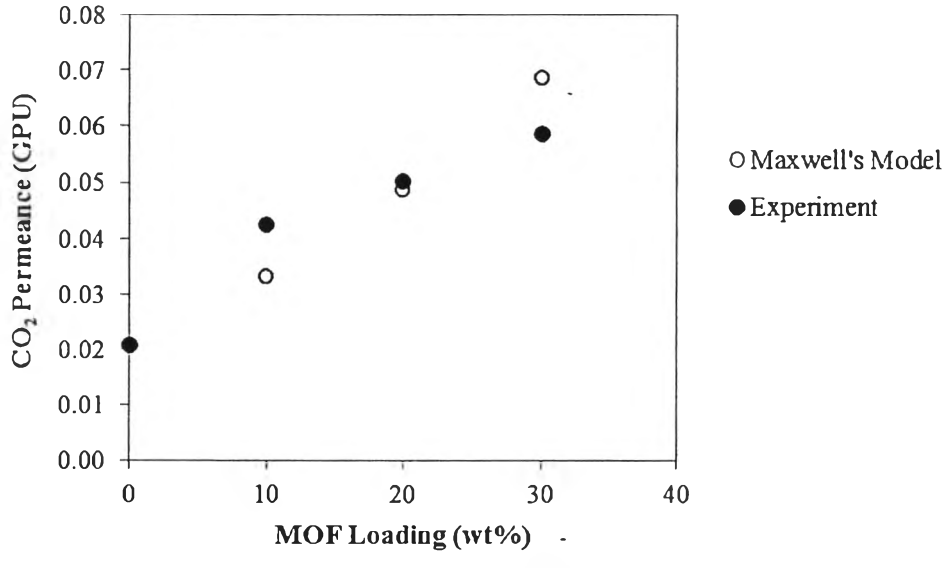

Figure 4.9 Comparison of CO_2 permeances of M199-U MMMs based on Maxwell model and experimental data at the pressure of 50 psi.

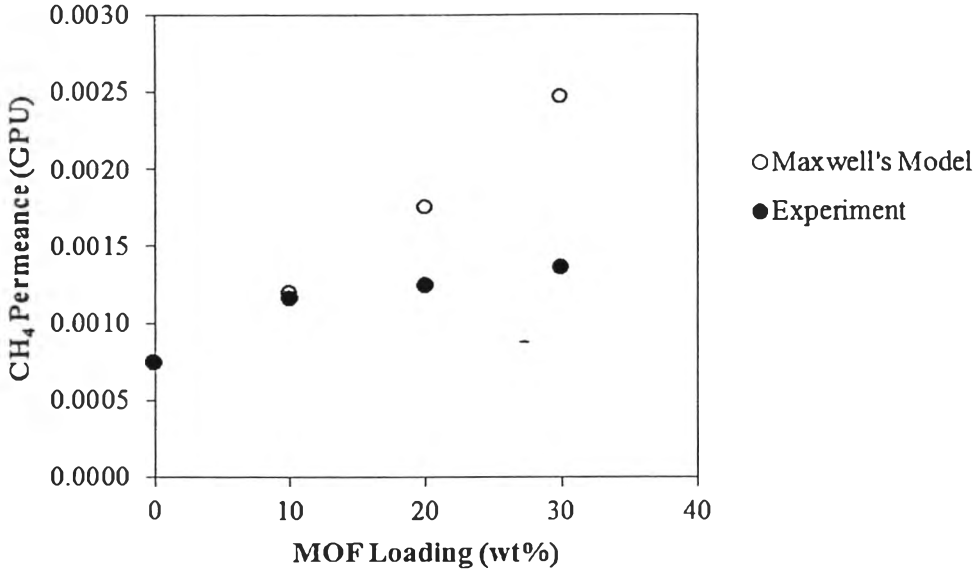

Figure 4.10 Comparison of CH_4 permeances of M199-U MMMs based on Maxwell model and experimental data at the pressure of 50 psi.

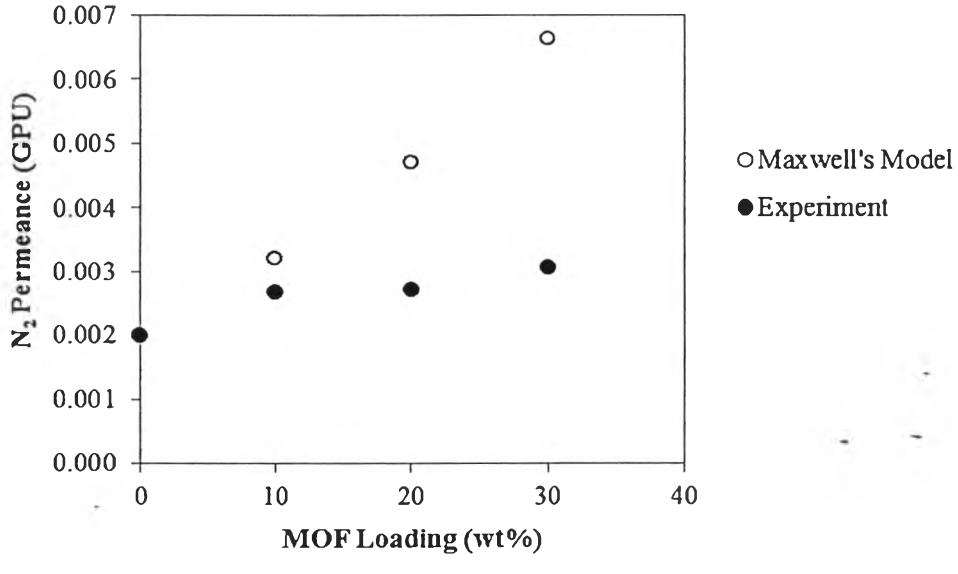

Figure 4.11 Comparison of N_2 permeances of M199-U MMMs based on Maxwell model and experimental data at the pressure of 50 psi.

As shown in Figure 4.9, using the P_{eff} calculated for different gases, the predicted CO_2 permeances of MOF-Ultem MMMs at different loadings matched rather well with the experiment data. On the other hand, CH_4 and N_2 permeances

appeared to be an underprediction and had larger difference from the Maxwell model at the higher MOF loading. It was hypothesized that the larger than predicted permeance could arise from both additional free volume contribution by MOF-199 and the agglomeration of some MOF-199 particles as evidented from SEM. Moreover, Song *et al.* (2012) also reported that the Maxwell model predictions matched well with the experimental data when the MOF loading was less than 20 wt%. The Maxwell model is only applicable to the dispersions that have low volume fraction (<20%) of dispersed particles because of the assumption that the flux pattern around a dispersed particle is not disturbed by the presence of other dispersed particles (Chung *et al.*, 2007).

For ZIF-Ultem, the CO_2, CH_4, and N_2 permeances obtained by the experiments and model are presented in Figures 4.12, 4.13, and 4.14, respectively.

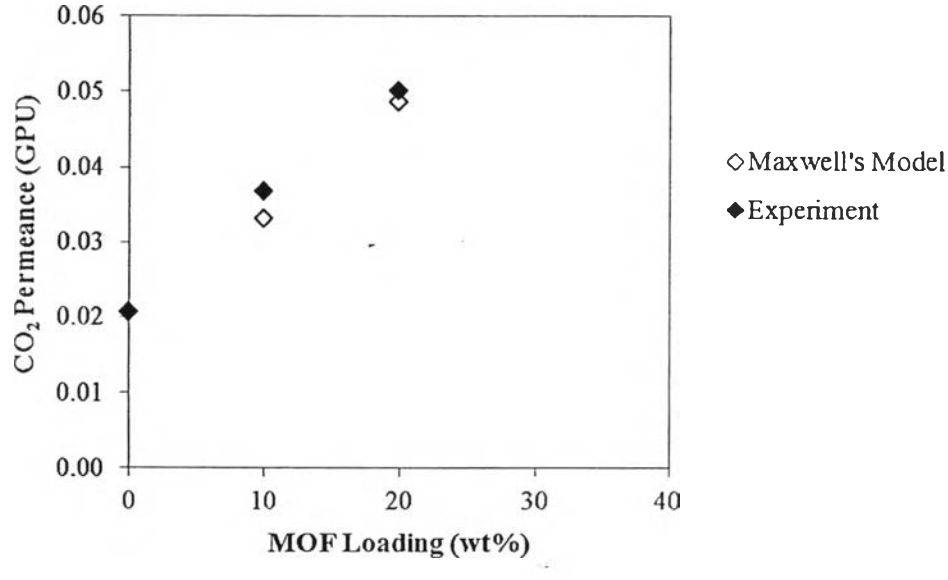

Figure 4.12 Comparison of CO_2 permeances of ZIF8-U MMMs based on Maxwell model and experimental data at the pressure of 50 psi.

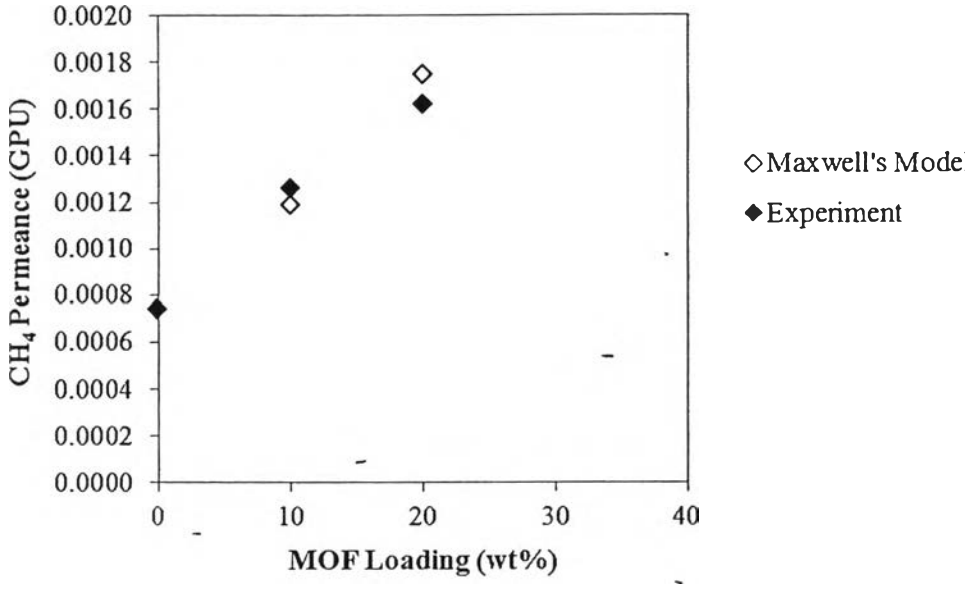

Figure 4.13 Comparison of CH_4 permeances of ZIF8-U MMMs based on Maxwell model and experimental data at the pressure of 50 psi.

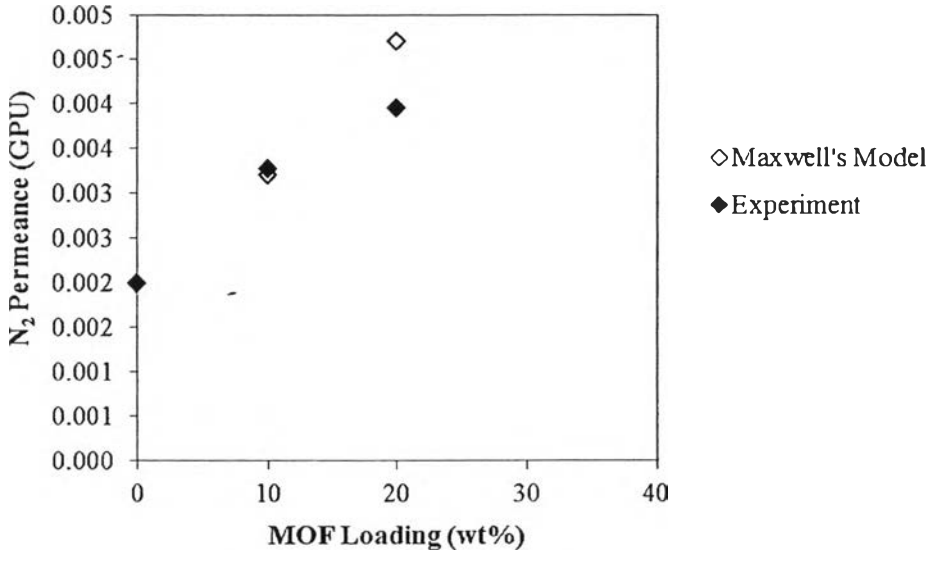

Figure 4.14 Comparison of N_2 permeances of ZIF8-U MMMs based on Maxwell model and experimental data at the pressure of 50 psi.

As discussed previously, since an increase in CO_2 permeance without an increase in CO_2/CH_4 selectivity of ZIF-Ultem with increasing ZIF-8 loading in the experiments might be due to the non-selective voids at ZIF-8 particles and polymer

interfaces; therefore, it is imperative to adopt that such phenomena would occur with ZIF-8 MMMs by comparing the gas permeances of these systems with those predicted from the Maxwell model. In comparison of gas permeance obtained from the experiments and by Maxwell model, the results showed that CO_2, CH_4, and N_2 permeances were generally increased with an increase in ZIF-8 loading. The results show that the experimental data of CO_2, CH_4, and N_2 permeances matched well with those of predicted by the Maxwell model, with a slightly higher for the experimental data than the Maxwell model predictions. This was due to the additional free volume contributed by ZIF-8 particles and also particle interaction where some small portions of ZIF-8 agglomerated together, allowing gas molecules to preferentially diffuse through these areas.